Biointerface Research in Applied Chemistry
Platinum Open Access Journal (ISSN: 2069-5837)

Article
Volume 12, Issue 2, 2022, 2586 - 2602
https://doi.org/10.33263/BRIAC122.25862602

Chemical Preparation, Crystal Structure Reinvestigation and Vibrational Study of $CoNa_3P_3O_{10}.12H_2O$ and X-ray Characterization of the New Anhydrous Triphosphate $CoNa_3P_3O_{10}$

El Mehdi Majdi [1,*], Mustafa Belhabra [1], Ali Ouasri [2], Ismail Fahim [1], Rachid Essehly [3], Said Belaaouad [1]

[1] Laboratory of Physical Chemistry of Materials, Faculty of Sciences Ben M'sick, Casablanca, Hassan II University of Casablanca, Morocco; majdielmehdismc@gmail.com (E.M.); mustapha.belhabra@gmail.com (M.B.); alfahimismail@yahoo.fr (I.F.); sbelaaouad@yahoo.fr (S.B.);
[2] Laboratoire (ReSIP), Centre Régional des Métiers de l'Education et de la Formation, Madinat Al Irfane, Souissi, BP 6210 Rabat, Morocco; aouasri@yahoo.fr (A.O.);
[3] Energy and Transportation Science Division, Oak Ridge National Laboratory, Oak Ridge, TN, 37830, USA; essehlir@ornl.gov (R.E.);
* Correspondence: majdielmehdismc@gmail.com (E.M.);

Scopus Author ID 57213164812
Received: 23.04.2021; Revised: 23.05.2021; Accepted: 27.05.2021; Published: 24.06.2021

Abstract: The triphosphate dodecahydrate of cobalt and sodium $CoNa_3P_3O_{10}.12H_2O$ was prepared by the ion exchange resin process. Its structure was studied by X-ray diffraction and determined in the monoclinic space group $P12_1/c1$with the unit-cell parameters a = 14.6650(5) Å, b=9.1916(3) Å, c = 15.0239(5) Å,β =90.2210(10) °, Z = 4 and V = 2025.13(12) $Å^3$. The thermal dehydration of this compound was performed, leading to an anhydrous new form, $CoNa_3P_3O_{10}$, which was characterized by X-ray diffraction. The obtained $CoNa_3P_3O_{10}$ crystallized in monoclinic space group P21/n with the unit-cell parameters a=15,3774 Å, b=7,6988 A°, c=14,2832A°, β=92,9115°.The characteristic IR wavenumbers of the $P_3O_{10}^{5-}$ ions observed in the vibrational spectra were calculated using isotopic substitutions, which confirms the existence of these groups in the studied compound. A comparison between the IR and Raman wavenumbers of $CoNa_3P_3O_{10}.12H_2O$, $CoNa_3P_3O_{10}$ and $Na_5P_3O_{10}.12H_2O$ was performed. A kinetic study was also made for $CoNa_3P_3O_{10}·12H_2O$.

Keywords: Triphosphate; X-ray diffraction; nfrared; Raman; spectroscopy sotopic ubstitution; dehydration; kinetic.

1. Introduction

Phosphates containing $P_nO_{3n+1}^{(n+2)-}$ (n = 1, 2 and 3) polyanions have been intensively studied over the last decades due to their applications in various fields: solid electrolytes for energy storage, Li-ion batteries, ceramics, luminescence and magnetism [1-5]. The Kanonerovite, $MnNa_3P_3O_{10}.12H_2O$, is a natural triphosphate mineral [6] and other synthetic triphosphates were reported in the literature: $CuNa_3P_3O_{10}.12H_2O$ [7], $Gd_5(P_3O_{10})_3.22H_2O$ and $Er_5(P_3O_{10})_3.20H_2O$ [8], $Zn2NaP_3O_{10}.9H_2O$ [9], and $CdNa_3P_3O_{10}.12H_2O$ [10]. $(NH_3C_6H_4COOH)_3H_2P_3O_{10}.3H_2O$ [11].

Anhydrous triphosphates have also been studied: $NaMn_6(P_3O_{10})(P_2O_7)$ [12], $TlFeHP_3O_{10}$ [13], $Ca_{0.5}FeHP_3O_{10}$ [14], $Sr_3ClP_3O_{10}$ [15], $Ca(OH)_2$-$Na_5P_3O_{10}$-Ce-Cl_3 [16].

These last ternary phosphates, with associated [PO_4] and [MO_6] frameworks, are efficiently used for waste storage hosts [17].

In the present work, we deal with the structural study of the hydrated $CoNa_3P_3O_{10}.12H_2O$ prepared by the resin exchange method and the characterization by X-ray diffraction of the new anhydrous phase $CoNa_3P_3O_{10}$ obtained from the thermal dehydration of $CoNa_3P_3O_{10}.12H_2O$.

The vibrational studies, thermal, kinetic behavior, and IR frequencies calculated for the $P_3O_{10}^{5-}$ion by isotopic substitutions are developed here in order to collect the maximum information on the structural and vibrational relationships and the reactivity of condensed phosphates of triphosphates with sodium $CoNa_3P_3O_{10}.12H_2O$ and anhydrous triphosphate $CoNa_3P_3O_{10}$. A kinetic study was carried out for the compound $CoNa_3P_3O_{10}.12H_2O$.

2. Materials and Methods

2.1. Chemical reparation.

Most well-characterized condensed phosphates were prepared in two steps: the first one was the preparation of the condensed phosphate acid $H_5P_3O_{10}$, and the second step was the elaboration of $CoNa_3P_3O_{10}.12H_2O$.

The triphosphoric acid $H_5P_3O_{10}$ used in this reaction was prepared from an aqueous solution of $Na_5P_3O_{10}$ passed through an ion-exchange resin, "Amberlite IR 120" [18]. The solution passage rate through the cation exchanger was 2mL/min, according to the first step of the chemical reaction:

$$Na_5P_3O_{10} \rightarrow \quad H_5P_3O_{10}$$

The polycrystalline $CoNa_3P_3O_{10}.12H_2O$ was prepared by slowly adding dilute triphosphoric acid $H_5P_3O_{10}$ to an aqueous solution of cobalt carbonate and sodium carbonate, according to the second step chemical reaction:

$$H_5P_3O_{10} + CoCO_3 + 3/2\ Na_2CO_3 + 19/2\ H_2O \rightarrow \quad CoNa_3P_3O_{10}.12H_2O + 5/2\ CO_2$$

The preliminary obtained solution was then slowly evaporated at room temperature for several weeks until polycrystalline samples of $CoNa_3P_3O_{10}.12H_2O$ were obtained.

The anhydrous phase $CoNa_3P_3O_{10}$ was obtained by total thermal dehydration of $CoNa_3P_3O_{10}.12H_2O$, between 400 and 500 °C, and is a new anhydrous triphosphate of cobalt and sodium.

$$CoNa_3P_3O_{10}.12H_2O \quad \rightarrow \quad CoNa_3P_3O_{10} + 12H_2O$$

2.2. X-ray iffraction, crystal data, intensity data collection and structure.

The X-ray single-crystal structure analysis was obtained using a Bruker X8 APEX S Diffractometer at room temperature. This is a 4-circle diffractometer (50 kV, 50 mA) equipped with a Mo radiation source Kα (λ = 0.71073Å). The data reduction, determination of the space group and refinement of the parameters of the elementary cell were performed using the SAINT-Plus software. The analytical absorption correction was applied using Multi-scan software [19]. The structure was solved by direct methods using the SHELXL2014 program [20]. The refinement of the structure was carried out by SHELXL 2016 [21]. The final

refinement of atomic positions and parameters of anisotropic thermal displacements R = 0.0436, wR = 0.0592 for 7084 reflections satisfying criterion I ≥ 2σ (I).

2.3. Fourier-Transform Infrared spectroscopy.

An ENTIR-27 FTIR spectrometer and Omnic software were used to record and characterize the infrared spectrum of triphosphate dodecahydrate of cobalt and sodium $CoNa_3P_3O_{10}.12H_2O$ between 400 and 4000 cm^{-1}. The conditions used to record the infrared absorption spectrum of this compound are as follows: 2 mg of product in 200 mg KBr are intimately related to the manufacture of a pellet at room temperature and at atmospheric pressure.

2.4. Raman spectroscopy.

The Raman spectrum was recorded in the range of 200-1400 cm-1 by a Raman dispersive microscope DXR2 (Thermo scientific 633 nm is a very strange wavelength for argon laser. Besides, 6 Mw is a huge power for gas lasers. Please test the parameters.

2.5. Thermal behavior.

The TGA-DTA coupled measurements were performed using a multimodule 92 Setaram analyzer operating from room temperature up to 800°C, in a platinum crucible, at various heating rates from 1 to 15°C.min^{-1}.

3. Results and discussion

3.1. Structure analysis.

The crystallographic data and refinement of the structure of $CoNa_3P_3O_{10}.12H_2O$ are given in table 1. The final atomic positions and anisotropic thermal parameters for the $CoNa_3P_3O_{10}.12H_2O$ structure are given in Tables 2 and 3, respectively.

Table 1. Crystallographic data and refinement of the structure of $CoNa_3P_3O_{10}.12H_2O$

I. Crystal data	
Formula	$CoNa_3P_3P_{10}.12H_2O$
formula weight	597.00 $g.mol^{-1}$
Crystal system	Monoclinic
Space group	P 1 $2_1/C_1$ (no. 14)
a (Å)	14.6650(5)
b (Å)	9.1916(3)
c (Å)	15.0239(5)
α=γ(°)	90
β(°)	90.2210(10)
V ($Å^3$)	2025.13(12)
Z	4
ρχαλ.	1.958 γ. χμ^{-3}
Absorption coefficient μ (mm^{-1})	1.248
Size/color	0.296 x 0.043 x 0.037/ clear light pink
Temperature (°K)	150
Wavelength (Mo Kα) (Å)	0.71073
Theta range (°)	2.598°-31.651
II. Intensity measurement	
Diffractometer	Bruker Kappa APEX II
Index limits	-21≤ h ≤ 21 , −13 ≤ k ≤ 13 , −13 ≤ l ≤13
Reflections collected	9879
Number of independent reflections	5602

Total number of reflections	7084 I > 2σ(I)
III. Structure determination	
Goodness-of-fit on F2	(Δ/ρ) max.= 1.113
Absorption correction	SHELXL-97 ShelXle /ShelXl-97
Refined parameters	111
Final index R for all data	R1 = 0.0436, Rw2 = 0.0592
Final R indexes [I>=2 σ (I)]	R1 = 0.0255, Rw2 = 0.0541

3.2. Structure description.

The Cobalt sodium triphosphate dodecahydrate $CoNa_3P_3O_{10}.12H_2O$ crystallized in the monoclinic system, space group $P12_1/c1$, with the following unit cell parameters: a = 14.6650(5) Å, b = 9.1916 (3) Å, c = 15. 0239 (5) Å, β =90.2210 (10) °, Z = 4 and V = 2025.13(12) $Å^3$.

The unit-cell of $CoNa_3P_3O_{10}.12H_2O$ contains four $P_3O_{10}^{5-}$ anions, each of which consists of three crystallographically independent P(1)O4, P(2)O4 and P(3)O4 tetrahedra. The three tetrahedra have no special characteristics. The $P_3O_{10}^{5-}$ anion observed in the structure of this compound has no internal symmetry. The cohesion between the anions $P_3O_{10}^{5-}$ is ensured via the associated cations Na^+ and Co^{2+}. The main geometrical characteristics of the three P(1)O4, P(2)O4 and P(3)O4 tetrahedra of the $P_3O_{10}^{5-}$ anion are quite similar to those observed generally in triphosphates.

The crystal structure of this compound consists of slabs parallel to the plane of the bc plane (Figure 1), which results from the cohesion of two types of metal chains, C1 and C2 (Figure 2). The C1 chain consists of octahedra [Na(2)O_6], sharing the O15-O16 edge (water molecules) with the strongly deformed tetragonal pyramid [Na (3)O5]. These dimmers share a corner O5 (oxygen from P2). In the C2 chain, the octahedra [Na(1)O_6] and [MO_6] share the O6 (oxygen from P2), O12 (water) and O19 (water) sides, and they are also connected by an O11 (water) wedge. Details of the connection between chains C1 and C2 via the O-P-O bridges of the P_3O_{10} phosphate groups are shown in Figures 3 and 4.Table 4 should be described in the text before Table 5. The octahedra [CoO6] are not directly connected in the structure, and the shortest distances of Co-Co are 5.069(6) Å. The phosphorus atoms (P^{VI}) occupy three symmetrically independent positions coordinated tetrahedrally. The [PO_4] share a vertex to form the triphosphate P_3O_{10} polyanions. The average distances P-O in P(1)O4, P(2)O4 and P(3)O4 are 1.5292, 1.5404 and 1.5423 A, respectively (see Table 4 for details), which are of the same magnitude as the values reported in $CuNa_3P_3O_{10}.12H_2O$ [22] and $CdNa_3P_3O_{10}.12H_2O$ [23]. P_3O_{10} could be considered as a combination of two P_2O_7 groups, characterized by the angles P-O-P 133.61(14) and 132.02(13), and the phosphate group P_3O_{10} acts differently on metals, being monodentate and tridentate with respect to the coordination of Na and Co

Table 2. Atomic coordinates and isotropic displacement parameters (in $Å^2$).

Atoms	X	Y	Z	U
Co01	0.75186(2)	0.54466(2)	0.67902(2)	0.00628(4)
P002	0.74143(2)	0.65696(4)	0.48227(2)	0.00680(6)
P003	0.89073(2)	0.77884(4)	0.59110(2)	0.00672(6)
P004	0.59546(2)	0.76972(4)	0.59677(2)	0.00663(6)
Na05	0.85745(4)	0.53450(6)	0.29097(4)	0.01209(11)
Na06	0.75386(4)	0.26630(6)	0.56368(4)	0.01235(11)
Na07	0.61342(4)	0.69162(7)	0.29723(4)	0.01751(13)
O008	0.64819(6)	0.69480(10)	0.67079(6)	0.00959(18)
O009	0.85459(6)	0.69597(10)	0.67179(6)	0.00893(18)
O00A	0.75140(7)	0.55542(11)	0.81973(7)	0.00976(18)
O00B	0.75252(7)	0.52260(10)	0.53739(6)	0.00972(18)

Atoms	X	Y	Z	U
O00C	0.90232(6)	0.93897(10)	0.61063(6)	0.01012(18)
O00D	0.84917(7)	0.37108(11)	0.67968(7)	0.01019(19)
O00E	0.66041(7)	0.36894(11)	0.67886(7)	0.00973(18)
O00F	0.97325(7)	0.70710(11)	0.55152(7)	0.0124(2)
O00G	0.59621(7)	0.93284(10)	0.60671(6)	0.01029(18)
O00H	0.50483(7)	0.58409(13)	0.39372(7)	0.0138(2)
O00I	0.50111(6)	0.70721(11)	0.58070(7)	0.01091(19)
O00J	0.87089(7)	0.15034(13)	0.48413(7)	0.0139(2)
O00K	0.74619(7)	0.64759(11)	0.38393(6)	0.01098(19)
O00L	0.64466(7)	0.13245(12)	0.48371(7)	0.0137(2)
O00M	0.98340(7)	0.56620(12)	0.39006(7)	0.0136(2)
O00N	0.64695(6)	0.73429(11)	0.50348(6)	0.01107(19)
O00O	0.81183(7)	0.77722(11)	0.51530(7)	0.0139(2)
O00P	0.87933(8)	0.76396(12)	0.22199(8)	0.0148(2)
O00Q	0.51267(8)	0.89288(13)	0.28276(8)	0.0156(2)
O00R	0.56943(9)	0.51181(13)	0.18819(8)	0.0179(2)
O00S	0.80368(8)	0.29581(12)	0.32474(8)	0.0150(2)
O00T	0.77700(9)	0.47059(14)	0.15797(8)	0.0232(3)
H00A	0.7063(15)	0.517(2)	0.8381(14)	0.027(6)
H00C	0.9022(13)	0.384(2)	0.6624(12)	0.016(5)
H00G	0.9159(14)	0.765(2)	0.1842(14)	0.025(5)
H00O	0.9186(15)	0.193(2)	0.4761(14)	0.031(6)
H00K	0.7491(14)	0.287(2)	0.3146(13)	0.023(5)
H00Q	0.6226(14)	0.066(2)	0.5159(15)	0.031(6)
H00S	0.9775(14)	0.616(2)	0.4371(15)	0.032(6)
H00E	0.6545(13)	0.317(2)	0.7250(14)	0.023(5)
H00B	0.7971(15)	0.511(2)	0.8422(14)	0.033(6)
H00T	0.9976(14)	0.487(2)	0.4065(14)	0.028(6)
H00R	0.6004(14)	0.177(2)	0.4666(13)	0.021(5)
H00D	0.8543(14)	0.314(2)	0.7230(14)	0.029(6)
H00L	0.8145(15)	0.252(2)	0.3707(15)	0.036(6)
H00M	0.5056(15)	0.499(3)	0.4020(15)	0.033(6)
H00U	0.7577(16)	0.391(3)	0.1435(16)	0.043(7)
H00W	0.4749(16)	0.880(3)	0.2491(16)	0.041(7)
H00X	0.4912(15)	0.944(3)	0.3241(16)	0.040(7)
H00V	0.7945(15)	0.511(3)	0.1151(16)	0.033(6)
H00H	0.8941(13)	0.835(2)	0.2562(14)	0.026(5)
H00F	0.6110(16)	0.382(3)	0.6584(15)	0.039(7)
H00P	0.8820(16)	0.084(3)	0.5142(16)	0.040(7)
H00I	0.5172(17)	0.522(3)	0.1674(16)	0.043(7)
H00N	0.5056(14)	0.621(2)	0.4453(15)	0.034(6)
H00J	0.6001(18)	0.521(3)	0.1518(17)	0.045(8)

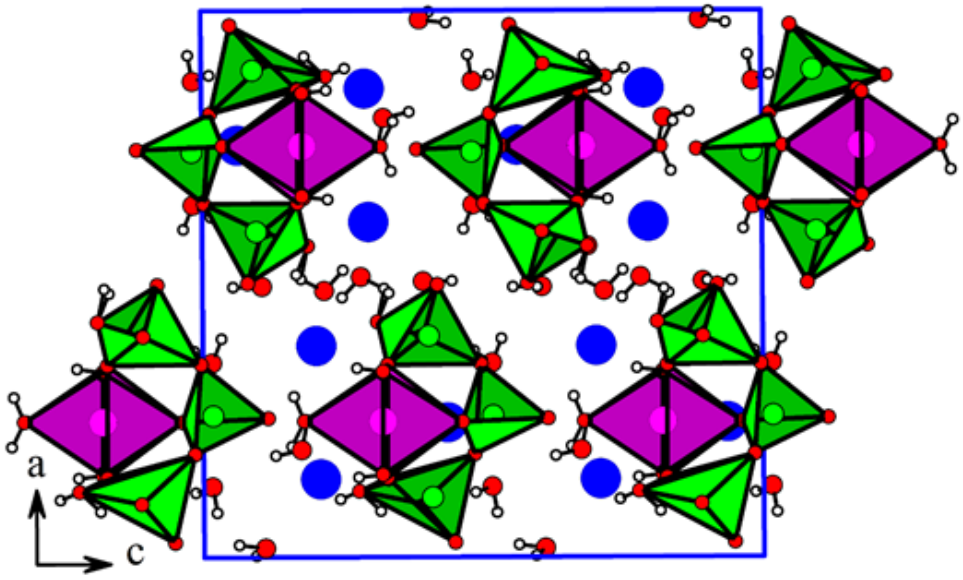

Figure 1. The coordination of the cobalt atom in $CoNa_3P_3O_{10}\cdot 12H_2O$.

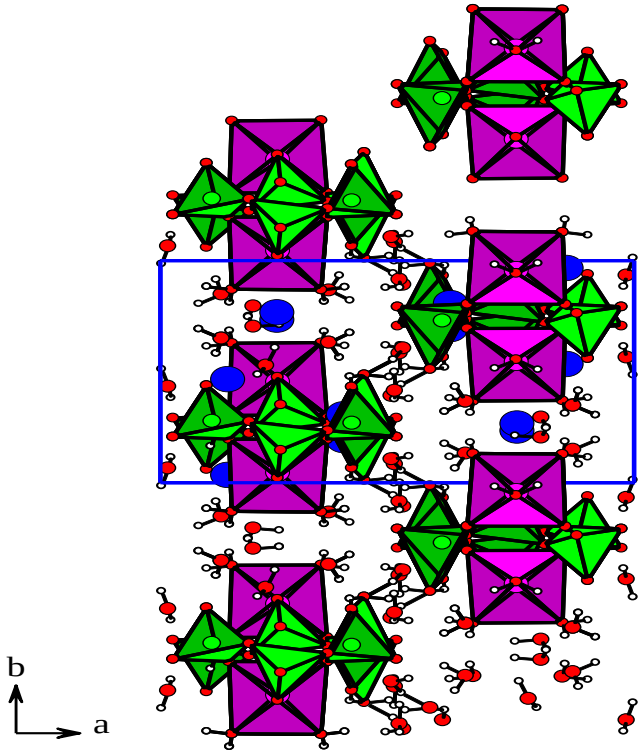

Figure 2. The coordination of the cobalt atom in $CoNa_3P_3O_{10}\cdot 12H_2O$.

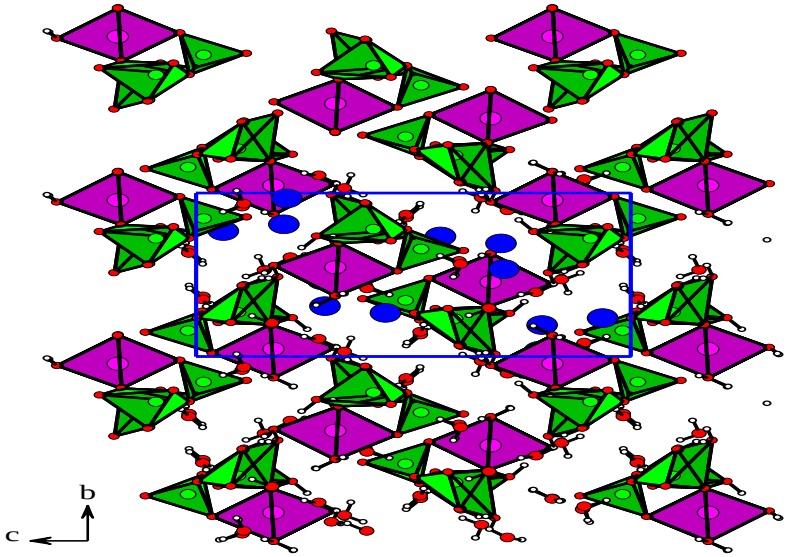

Figure 3. Projection of PO_4 and CoO_6 polyhedra along axes a, b and c in $CoNa_3P_3O_{10}.12H_2O$.

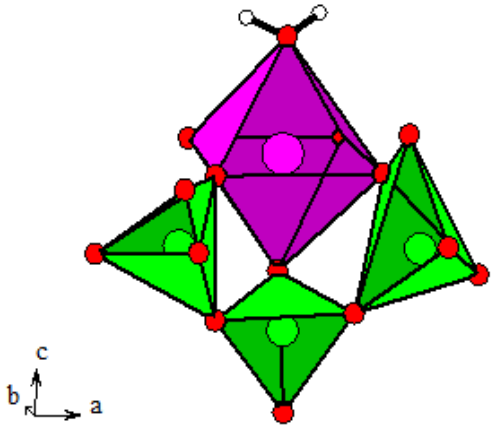

Figure 4. The coordination of the natrium atom in $CoNa_3P_3O_{10}.12H_2O$.

Table 3. Anisotropic displacement parameters (in Å^2)

Atom	U11	U22	U33	U23	U13	U12
Co01	0.00694(8)	0.00599(8)	0.00591(8)	0.00043(6)	0.00000(6)	-0.00015(6)
P002	0.00707(14)	0.00792(15)	0.00540(14)	0.00007(11)	0.00019(11)	0.00006(12)
P003	0.00656(14)	0.00668(15)	0.00693(15)	0.00012(11)	0.00008(11)	-0.00094(11)
P004	0.00617(14)	0.00698(14)	0.00672(14)	-0.00017(11)	-0.00003(11)	0.00062(11)
Na05	0.0131(3)	0.0118(3)	0.0114(3)	-0.0008(2)	0.0011(2)	0.0001(2)
Na06	0.0130(3)	0.0112(3)	0.0129(3)	-0.0031(2)	0.0003(2)	0.0003(2)
Na07	0.0131(3)	0.0226(3)	0.0167(3)	0.0068(2)	-0.0012(2)	0.0000(2)
O008	0.0099(4)	0.0112(4)	0.0076(4)	0.0005(3)	-0.0002(3)	0.0029(4)
O009	0.0097(4)	0.0096(4)	0.0075(4)	0.0015(3)	0.0001(3)	-0.0020(3)
O00A	0.0090(4)	0.0107(4)	0.0095(4)	0.0016(4)	0.0000(4)	-0.0003(4)
O00B	0.0142(5)	0.0079(4)	0.0070(4)	0.0001(3)	0.0001(3)	0.0007(4)
O00C	0.0110(4)	0.0074(4)	0.0119(5)	-0.0005(3)	0.0002(4)	-0.0011(3)
O00D	0.0090(5)	0.0107(5)	0.0109(5)	0.0029(4)	-0.0001(4)	0.0010(4)
O00E	0.0094(5)	0.0101(5)	0.0097(5)	0.0030(4)	-0.0006(4)	-0.0014(4)
O00F	0.0108(5)	0.0114(5)	0.0150(5)	-0.0015(4)	0.0048(4)	0.0002(4)
O00G	0.0132(5)	0.0070(4)	0.0107(4)	-0.0007(3)	-0.0001(4)	0.0001(3)
O00H	0.0163(5)	0.0114(5)	0.0135(5)	0.0020(4)	-0.0033(4)	-0.0029(4)
O00I	0.0079(4)	0.0107(4)	0.0141(5)	0.0007(4)	-0.0006(4)	-0.0008(4)
O00J	0.0105(5)	0.0160(5)	0.0153(5)	0.0052(4)	0.0017(4)	-0.0005(4)
O00K	0.0119(5)	0.0155(5)	0.0056(4)	-0.0001(4)	0.0010(3)	0.0021(4)
O00L	0.0128(5)	0.0141(5)	0.0142(5)	0.0040(4)	-0.0023(4)	0.0007(4)
O00M	0.0157(5)	0.0130(5)	0.0121(5)	-0.0011(4)	0.0007(4)	0.0026(4)
O00N	0.0100(4)	0.0164(5)	0.0068(4)	0.0005(4)	0.0009(3)	0.0043(4)
O00O	0.0149(5)	0.0135(5)	0.0132(5)	0.0060(4)	-0.0070(4)	-0.0068(4)
O00P	0.0161(5)	0.0151(5)	0.0134(5)	-0.0020(4)	0.0035(4)	-0.0033(4)
O00Q	0.0144(5)	0.0172(5)	0.0152(5)	-0.0021(4)	0.0003(4)	0.0016(4)
O00R	0.0126(5)	0.0208(6)	0.0204(6)	0.0064(5)	0.0004(5)	0.0006(4)
O00S	0.0139(5)	0.0153(5)	0.0157(5)	0.0036(4)	-0.0001(4)	0.0004(4)
O00T	0.0367(7)	0.0190(6)	0.0139(6)	-0.0012(5)	-0.0008(5)	-0.0076(5)

Table 4. Selected geometric parameters (Å°).

Co-O2	2,061(2)	P1-O3	1,510(2)
Co-O6	2,141(2)	P1-O4	1,619(2)
Co-O9	2,060(2)	P2-O4	1,594(2)
Co-O11	2,116(2)	P2-O5	1,479(2)
Co-O12	2,098(2)	P2-O6	1,495(2)
Co-O19	2,142(2)	P2-O7	1,594(2)
P1-O1	1,505(2)	P3-O7	1,624(2)
P1-O2	1,523(2)	P3-O8	1,506(2)
Co-O2-O6	90,35(8)	P1-O1-O2	112,1(1)
Co-O2-O9	94,87(8)	P1-O1-O3	114,5(1)
Co-O2-O11	91,45(8)	P1-O1-O4	107,0(1)
Co-O2-O12	171,96(8)	P1-O2-O3	111,7(1)
Co-O2-O19	91,01(8)	P1-O2-O4	107,7(1)
Co-O6-O9	90,43(8)	P1-O3-O4	103,0(1)
Co-O6-O11	177,32(8)	P2-O4-O5	109,1(1)
Co-O6-O12	85,90(8)	P2-O4-O6	109,1(1)
Co-O6-O19	85,98(8)	P2-O4-O7	100,9(1)
Co-O9-O11	91,40(8)	P2-O5-O6	120,0(1)
Co-O9-O12	92,27(8)	P2-O5-O7	105,5(1)
Co-O9-O19	173,13(8)	P2-O6-O7	110,5(1)
Co-O11-O12	92,07(8)	P3-O7-O8	106,5(1)
Co-O11-O19	91,99(8)	P3-O7-O9	107,8(1)
Co-O12-O19	81,64(8)	P3-O7-O10	102,3(1)
P3-O8-O7	106,5(1)		
P3-O8-O9	112,2(1)		
P3-O8-O10	113,4(1)		
P3-O9-O10	113,8(1)		

Table 5. Bond lengths (A°) and angles (°) in hydrogen-bonding scheme for $CoNa_3P_3O_{10}.12H_2O$.

	D–H	H···A	D–A	D–H···A
O11–H11A··· O8^i	0.82(3)	1.92(3)	2.741(3)	174(3)
O11–H11B··· O3^i	0.82(3)	1.90(3)	2.707(3)	169(3)
O12–H12A··· O2^i	0.82(3)	1.95(3)	2.763(3)	169(3)

	D–H	H···A	D–A	D–H···A
O12–H12B··· O20^{i}	0.823(19)	1.87(2)	2.685(3)	171(3)
O13–H13B··· O10^{ii}	0.83(3)	1.95(3)	2.768(3)	172(3)
O14–H14A··· O1^{ii}	0.82(2)	1.95(2)	2.757(3)	167(3)
O14–H14B··· O1	0.83(2)	1.92(2)	2.735(3)	169(4)
O17–H17A··· O3^{i}	0.82(3)	1.95(3)	2.756(3)	171(3)
O17–H17B··· O1^{iii}	0.82(3)	1.87(3)	2.691(3)	174(4)
O19–H19A··· O9^{i}	0.82(2)	1.96(2)	2.773(3)	171(4)
O19–H19B··· O14^{iv}	0.820(19)	1.91(2)	2.728(3)	174(3)
O20–H20B··· O10^{v}	0.822(14)	1.893(14)	2.712(3)	174(4)

3.3. Chemical stability.

The triphosphate dodecahydrate of cobalt and sodium $CoNa_3P_3O_{10}.12H_2O$ is stable under the normal temperature, till 50°C, and pressure conditions. As this is stated by IR spectrometry, X-ray diffraction and thermogravimetric analyses, the stability of $CoNa_3P_3O_{10}.12H_2O$ was observed during five months. However, after five months, the $CoNa_3P_3O_{10}\cdot12H_2O$ becomes not stable. This instability can be explained by the fact that four of the water molecules are zeolitic [24]. The X-ray diffraction pattern of $CoNa_3P_3O_{10}.12H_2O$ is shown in Figure 5.

3.4. Characterization by Infrared and Raman spectrometry and calculated IR frequencies for the $P_3O_{10}^{5-}$ by isotopic substitutions.

The infrared spectrum (Figure 6) of the powdered sample of $CoNa_3P_3O_{10}.12H_2O$ was studied in the range of 4000–400 cm^{-1}. The band assignments for the fundamental modes of stretching and bending of $P_3O_{10}^{5-}$ anions are presented in Table 6. The wavenumbers of the $P_3O_{10}^{5-}$ anion are assigned based on the characteristic vibrations of the P–O–P bridge, PO2 and PO3 groups. As the P–O bond in the PO2 and PO3 group is weaker than that in the P–O–P bridge, the vibrational wavenumbers of PO2 and PO3 are expected to be higher than those of P–O–P. The bands due to the symmetric and antisymmetric-stretching vibrations of PO2 and PO3 in $P_3O_{10}^{5-}$ are generally observed in the region of 1190–1010 cm-1 [25,26]. The bands observed in the domain 970–840 cm^{-1} are attributed to the antisymmetric and symmetric POP stretching modes. The bands due to δ(OPO), δ(PO_2), δ(PO_3) and δ(POP) are also identified and listed in Table 6. The wavenumbers obtained for the $P_3O_{10}^{5-}$ ion are comparable with those observed in the infrared spectra of $MNa_3P_3O_{10}.12H_2O$ (M= Cu and Ni) [26-28]. To note that IR frequencies and intensities were calculated for $P_3O_{10}^{5-}$ of exact symmetry C_1 for the substitutions of oxygen by the isotope ^{18}O and phosphorus by the ^{31}P isotope.

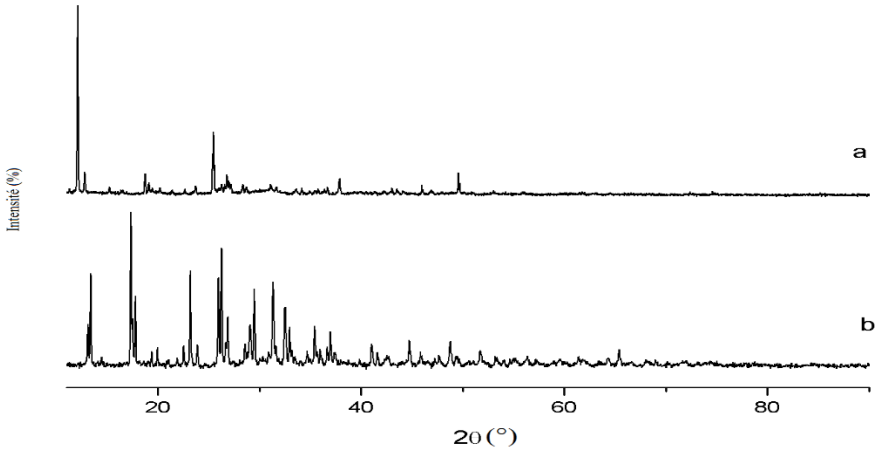

Figure 5. X-ray diffraction patterns of the phosphates (**a**) $CoNa_3P_3O_{10}.12H_2O$; (**b**) $CoNa_3P_3O_{10}$.

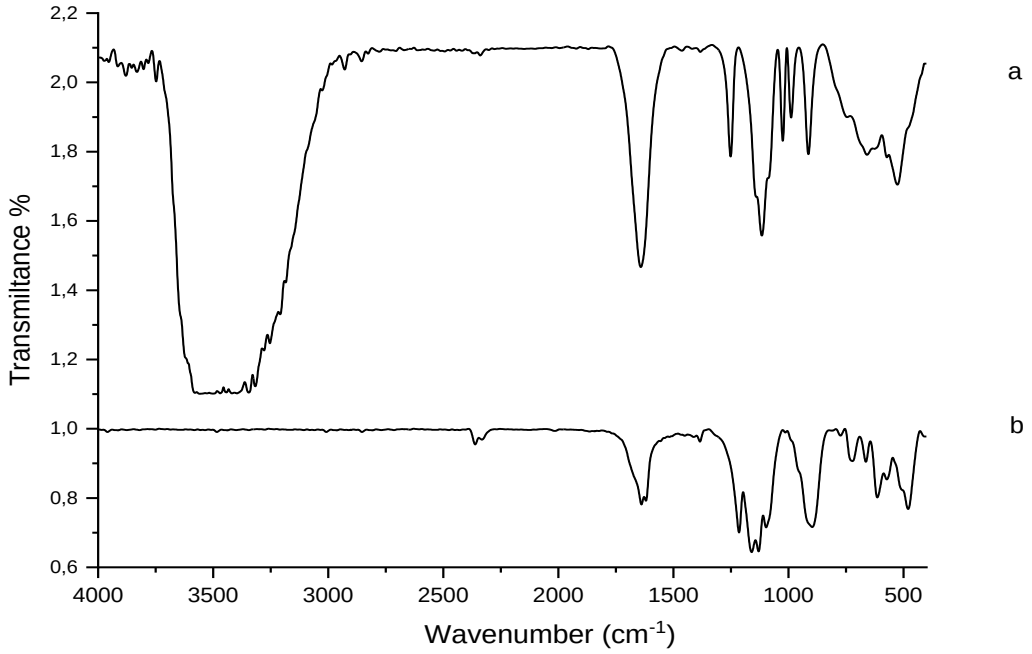

Figure 6. IR spectra of the phosphates (**a**) $CoNa_3P_3O_{10}.12H_2O$; (**b**) $CoNa_3P_3O_{10}$.

The Raman spectrum (Figure 7) of a $CoNa_3P_3O_{10}.12H_2O$ sample was studied from 200 to 1400 cm^{-1}. The band corresponding to the fundamental modes of $P_3O_{10}^{-5}$ are presented in Table 6. The wavenumbers of $P_3O_{10}^{-5}$ are assigned based on the characteristic vibrations of the P-O-P bridge, groups PO2 and PO3. Since the P-O link in the PO2 and PO3 groups is weaker than that of the P-O-P bridge, the vibration wavenumbers of PO2 and PO3 should be higher than those of P-O-P. The bands due to the symmetric and the antisymmetric stretching vibrations of PO2 and PO3 in $P_3O_{10}^{-5}$ are generally observed at 1340-865 cm^{-1}. The bands at 402-840 cm^{-1} are attributed to the antisymmetric and symmetric stretching modes of POP. The bands due to νs (PO2), νas (PO2), νs(PO3), and νas(P-O-P) are classified in Table 6, which also contains the IR wavenumbers calculated for $P_3O_{10}^{-5}$ by the MNDO [29] method for $CoNa_3P_3O_{10}.12H_2O$. The IR frequencies of the $P_3O_{10}^{-5}$ anions observed in the sodium cobalt dodecahydrate, $CoNa_3P_3O_{10}.12H_2O$, are close to those calculated.

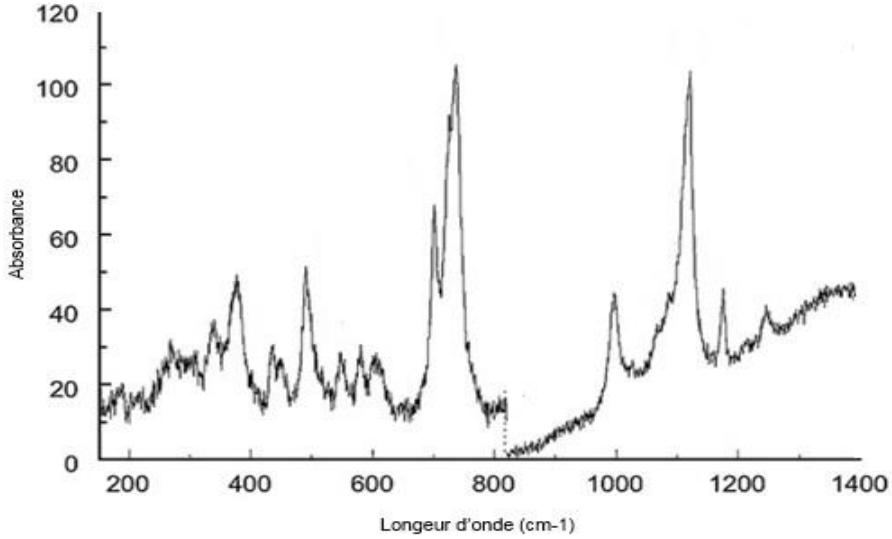

Figure 7. Raman spectra of the phosphates (a) $CoNa_3P_3O_{10}\cdot 12H_2O$.

Table 6. Assignments of the IR and Raman frequencies of $CoNa_3P_3O_{10}$ and $CoNa_3P_3O_{10}.12H_2O$.

$Na_5P_3O_{10}$ ν (observed) [26]	$CoNa_3P_3O_{10}.12H_2O$ ν (observed)		$CoNa_3P_3O_{10}$ ν (observed)	ν (calculated)	Vibration [30-32]
IR	IR	Raman	IR		
3442	3480	-			ν O-H
2920 2355		2870 2811	-		
1641	1638		-		ν_δ H-O-H
		1542	-		
1462		1392	1392		
1386		1379		1319	ν P=O
				1252	νas PO_2
1301	1252	1240		1249	νas PO_2
			1216		
	1116	1009	1158	1170	νas PO_3
			1095	1081	νs PO_2
1095	1021	1013		1059	νs PO_3
	983	970		962	νas POP
	918	900			
910			908	891	ν as POP
	851	830			
			727	724	νs POP
	657	670	663	671	νs POP
			615	605	δ PO_2
				560	δ PO_3
540			540	552	
510	524	490		537	
492				508	ν_{as} P-O-P
460			476	476	
450				466	
				433	

3.5. Thermal behavior.

The two curves corresponding to the TG and DTA analyses [33-37] in an air atmosphere at a heating rate of 10 °C min^{-1} of $CoNa_3P_3O_{10}.12H_2O$ are given in Figure 8.

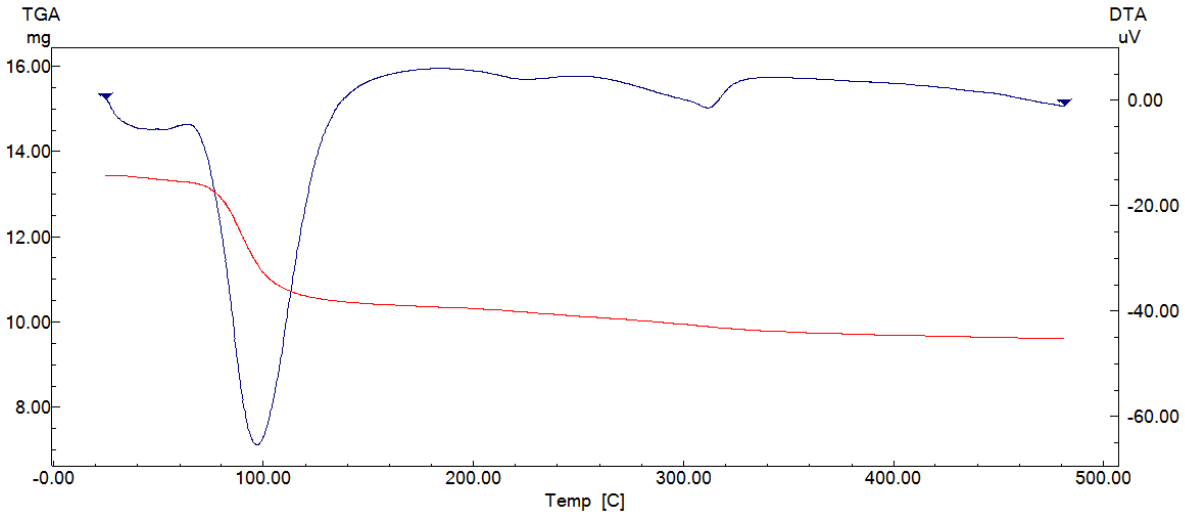

Figure 8. TGA-DTA curves of $CoNa_3P_3O_{10}.12H_2O$ at heat rate (10 °C min^{-1}).

The dehydration of the triphosphate dodecahydrate of cobalt and natrium $CoNa_3P_3O_{10}.12H_2O$ occurs in the temperature range 143-350°C, and corresponds to the elimination of 8 water molecules. The four other water molecules are of a zeolitic nature [24].

So, the thermal dehydration of $CoNa_3P_3O_{10}.12H_2O$ led to its new anhydrous form, $CoNa_3P_3O_{10}$, which is characterized by X-ray diffraction (Figure 5).

3.7. Step manner study.

The thermal behavior of $CoNa_3P_3O_{10}.12H_2O$ was studied in a step manner of temperature by X-ray diffraction and IR absorption spectrometry between 20 and 480 °C. X-ray diffraction patterns recorded after annealing for 36 hours at different temperatures reveal that $CoNa_3P_3O_{10}.12H_2O$ is stable up to 50°C.

The removal of twelve water molecules of hydration of $CoNa_3P_3O_{10}.12H_2O$, observed in the temperature range 60-160°C, destroyed the crystalline network and brings to an intermediate amorphous phase [38-40], which does not diffract the X-ray, nor exhibits the IR absorption bands characteristic of a triphosphate $P_3O_{10}^{5-}$. Between 400 and 500°C, the obtained X-Ray diffractogram (Figure 5) and IR spectrum (Figure 6), reveal the crystallization of a new phase which is nothing other than the anhydrous new form of triphosphate of the compound $CoNa_3P_3O_{10}.12H_2O$. So, the final product resulting from the dehydration of $CoNa_3P_3O_{10}.12H_2O$ between 400 and 500°C is the anhydrous new triphosphate $CoNa_3P_3O_{10}$.

The unit cell parameters were calculated for the anhydrous phase according to an automatic indexation using the computer program TREOR [41,42]. Subsequently, the structure was refined by the least-squares method using a computer program U-FIT [43]. $CoNa_3P_3O_{10}$ crystallizes in the monoclinic system, space group $P2_1/n$, Z = 2 with the unit-cell dimensions: a=15.3774 A° b=7.6988 A°, c=14.2832A°, α=90°, β=92.9115° γ=90°, M (20) = 80, F(20) = 93 (0.0028; 77) and V= 1465,58(0) $Å^3$.

The IR bands (Figure 6) and Raman peaks (Figure 7) of stretching and bending modes observed in the spectra of $CoNa_3P_3O_{10}$ are listed in Table 6. The IR and Raman spectra reveal that the transformation from the monoclinic dodecahydrate to the anhydrous phase takes place without any strong modification in the appearance of vibrational modes of the $P_3O_{10}^{5-}$ anions. $CoNa_3P_3O_{10}$ is stable until its melting point at 800°C.

3.8. Estimation of the thermodynamic functions.

Various equations of kinetic analyses are known, such as Kissinger's method [44], Kissinger-Akahira-Sunose (KAS) [45], Ozawa [46], Coats-Redfern [47] and Van Krevelen et al. [48] methods. Especially, the Ozawa and KAS equations were well described and widely used in the literature. Therefore, these methods are selected in studying the kinetics of thermal dehydration of the $CoNa_3P_3O_{10}.12H_2O$ compound. So, the water loss kinetic parameters were evaluated using the Kissinger-Akahira-Sunose (KAS) [45] and Ozawa [46] methods, from the curves $\ln(v/T^2m) = f(1/Tm)$ and $\ln(v) = f(1/Tm)$ (Figures 9 and 10), where v is the heating rate and Tm the sample temperature at the thermal effect maximum. The characteristic temperatures at maximum dehydration rates, T_m, for the triphosphate $CoNa_3P_3O_{10}.12H_2O$ are shown in Table 7. From these temperatures and according to the Kissinger - Akahira - Sunose (KAS) [45] and Ozawa [46] methods, the apparent activation energies of dehydration were calculated for the triphosphate $CoNa_3P_3O_{10}\cdot12H_2O$ (Table 8). For the Kissinger - Akahira - Sunose (KAS) [45] method, the slope of the resulting straight line of the curve: $\ln(v/T^2_m) = f(1/T_m)$ (Figure 9), equals to $-E_a/R$, which allows the apparent activation energy to be calculated (Table 7). Concerning the Ozawa [46] method, the slope of the resulting straight line on the curve: $\ln(v) = f(1/T_m)$ (Figure 10), equals -1.0516E/R, which also allows the apparent activation energy

(Table 8) to be calculated by this second way. The equations (1) and (2) corresponding to the two used methods, KAS [43]and OZAWA [46], are given, respectively, as followed:

$$\ln(\frac{\nu}{T^2_m}) = \ln(\frac{AR}{E}) - (\frac{E}{R})(\frac{1}{T_m}) \quad (1)$$

$$\ln \nu = \ln(\frac{AR}{1.0516E}) - 1.0516(\frac{E}{R})(\frac{1}{T_m}) \quad (2)$$

The pre-exponential factor or Arrhenius constant (A) can be calculated from both KAS [45] and Ozawa [46] methods. The related thermodynamic functions can be calculated using the activated complex theory (transition state) of Eyring [49,50]. The following general equation (3) can be written:

$$A = (\frac{e\chi k_B T_m}{h}) \exp(\frac{\Delta S^*}{R}) \quad (3)$$

Table 7. Characteristic temperatures at maximum dehydration rates, T_m in °K, at different heating rates from the DTA curves of $CoNa_3P_3O_{10}.12H_2O$.

Heating rate v (°C/min)	1	6	10	15
1st peak	358	365	369	373
1st peak	575	583	589	593

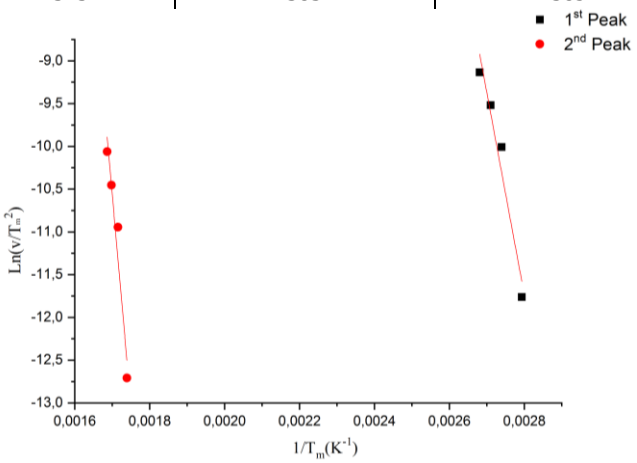

Figure 9. $Ln(v/T_m^2) = f(1/T_m)$ representation of the dehydration thermal effect of the triphosphate $CoNa_3P_3O_{10}.12H_2O$.

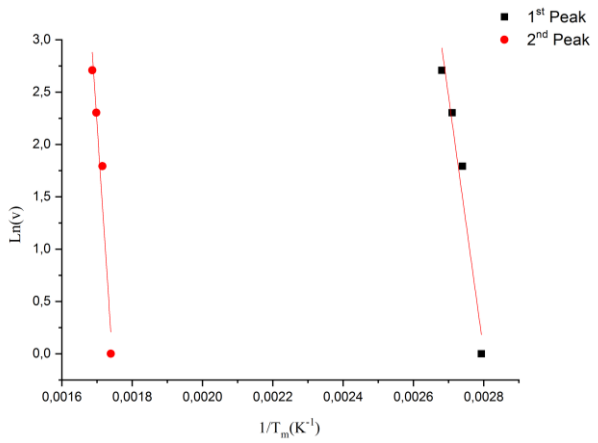

Figure 10. Ln(v) = f(1/Tm) representation of the dehydration thermal effect of the triphosphate $CoNa_3P_3O_{10}.12H_2O$.

Table 8. Activation energy values E_a, pre-exponential factor (A) and correlation coefficient (r^2) calculated by Ozawa and KAS methods for the dehydration of $CoNa_3P_3O_{10}.12H_2O$ under atmospheric pressure.

Model	**Ozawa method**	**KAS method**

	Ea (kJ.mol^{-1})	A. 10^6/min^{-1}	r^2	Ea (kJ.mol^{-1})	A /min^{-1}	r^2
1st peak	25,438	9,148*10^7	0,9996	20,153	59,079	0,9997
2st peak	25,623	3,193*10^7	0,9993	19,305	14,599	0,9993

Where e is the Neper number (e = 2.7183), χ is the transition factor, which is unity for the monomolecular reaction, K_B is the Boltzmann constant (K_B = 1.3806 × 10^{-23} J.K^{-1}), h is Plank's constant (h = 6.6261 × 10^{-34} J.s), T_m is the peak temperature of the DTA curve, R is the gas constant (R = 8.314 J.K^{-1}.mol^{-1}) and ΔS* is the entropy change of transition state complex or entropy of activation. Thus, the entropy of activation may be calculated by the equation (4) as follows:

$$\Delta S^* = R\ln(\frac{Ah}{e\chi k_B T_m}) \quad (4)$$

The enthalpy changes of transition state complex or heat of activation (ΔH*) and Gibbs free energy of activation (ΔG*) of decomposition were calculated according to the equations (5) and (6), respectively:

$$\Delta H^* = E^* - RT_m \quad (5)$$

$$\Delta G^* = \Delta H^* - \Delta S^* T_m \quad (6)$$

where, E* is the activation energy E_a of both KAS [45] and Ozawa [46] methods. The activation energy values are listed in Table 8. The thermodynamic functions were calculated from equations (4), (5) and (6) and summarized in Table 9. The negative values of ΔS* from two methods for the dehydration step reveal that the activated state is less disordered compared to the initial state.

These ΔS* values suggest many degrees of freedom due to rotation which may be interpreted as a « slow » stage [51] in this step. The positive values of ΔG* at all studied methods are because the dehydration processes are not spontaneous.

The positive ΔG* is controlled by a small activation entropy and large positive activation enthalpy according to equation 6. The endothermic peak in the DTA data agrees well with the positive sign of the activation enthalpy (ΔH*). The estimated thermodynamic functions ΔS* and ΔG* (Table 9) from two methods are different to some extent due to the different pre-exponential factor of about 10^6 as in the case of $CuNa_3P_3O_{10}.12H_2O$ [26] and ΔH* (Table 9) exhibits an independent behavior on the pre-exponential factor as seen from exhibiting nearly the same value.

Table 9. Values of ΔS*, ΔH* and ΔG* for dehydration step of $CoNa_3P_3O_{10}.12H_2O$ calculated according to Ozawa [46]and KAS [45] equations

Model	**Ozawa method**			**KAS method**		
	ΔS* J.K^{-1}.mol^{-1}	ΔH* kJ.mol^{-1}	ΔG* kJ.mol^{-1}	ΔS* J.K^{-1}.mol^{-1}	ΔH* kJ.mol^{-1}	ΔG* kJ.mol^{-1}
1st peak	-102,781	22,896	76,123	-242,279	14,612	101,302
2st peak	-116,849	13,475	78,301	-245,216	13,156	122,529

4. Conclusions

The dodecahydrate triphosphate of cobalt and sodium $CoNa_3P_3O_{10}.12H_2O$, obtained as single-crystals by the resin exchange method, crystallizes in the monoclinic system, space group $P12_1/C_1$, Z = 4, a = 7.6992(2) Å, b = 12.3237(3) Å, c = 11.8023 (3) Å and β= 101.181(5)°. The TG curve of $CoNa_3P_3O_{10}.12H_2O$ shows that dehydration takes place in one step between 70°C and 560°C. Four water molecules contained in $CoNa_3P_3O_{10}.12H_2O$ are of zeolitic nature. The total removal of the water at 560°C is followed by the crystallization of a new triphosphate $CoNa_3P_3O_{10}$. This anhydrous compound resulted from the total dehydration of $CoNa_3P_3O_{10}.12H_2O$ between 300°C and 560°C, crystallizes in the monoclinic system, space group $P2_1/n$, Z = 4, a=15.3774, A° b=7.6988 A°, c=14.2832A°, β=92.9115°.

The differential thermal analysis of $CoNa_3P_3O_{10}.12H_2O$ shows only one endothermic peak due to the dehydration of this compound. Using the DTA results, the kinetic study calculates the thermodynamic function E_a, ΔH, ΔS and ΔG by the KAS, and Ozawa methods.

The Raman and infrared spectra of $CoNa_3P_3O_{10}.12H_2O$ and $CoNa_3P_3O_{10}$ have been recorded and interpreted. The vibrational study of $CoNa_3P_3O_{10}.12H_2O$ allowed us to assign the IR and Raman bands observed in the triphosphate dodecahydrate. The presence of the frequencies characterizing $P_3O_{10}^{5-}$ in the vibrational spectra confirming the existence of the $P_3O_{10}^{5-}$ ion. A comparison of the Raman and infrared bands of the $CoNa_3P_3O_{10}.12H_2O$ compound, its anhydrous form $CoNa_3P_3O_{10}$, and $Na_5P_3O_{10}$ was performed.

Funding

This research received no external funding.

Acknowledgment

I want to thank all the authors and mainly my supervisor, Said Belaaouad, for the support necessary to carry out this work, and I would like to thank my father for his constant support, may God have mercy on him, and may God enlighten his face.

Conflicts of Interest

The authors declare no conflict of interest.

References

1. Zhao, J.; Zhao, D.; Xue, Y. L.; Zhong, Q.; Zhang, S. R.; Liu, B. Z. Novel Tantalum Phosphate $Na_{13}Sr_2Ta_2(PO_4)_9$: Synthesis, Crystal Structure, DFT Calculations and Dy3+-Activated Fluorescence Performance. *Acta Crystallogr. Sect. C Struct. Chem.* **2018**, *74*, 1045–1052, https://doi.org/10.1107/S2053229618011877.
2. Moutataouia, M.; Zambon, D.; Boyer, D.; Lamire, M.; El Ammari, L.; Mahiou, R. Crystallographic and Optical Properties of Eu^{3+} Doped $K_2Na_3P_3O_{10}$ Triphosphate. *J. Alloys Compd.* **2018**, *748*, 206–215, https://doi.org/10.1016/j.jallcom.2018.02.284.
3. Hou, Y.; Zhang, B.; Wu, H.; Yu, H.; Hu, Z.; Wang, J.; Wu, Y. $K_3B_4PO_{10}$ and $K_2MB_4PO_{10}$ (M = Rb/Cs): Rare Mixed-Coordinated Borophosphates with Large Birefringence. *Inorg. Chem. Front.* **2020**, https://doi.org/10.1039/D0QI01354D.
4. Iglesias, I.; Alfonso, B. F.; Amghouz, Z.; Trobajo, C.; García, J. R.; Huidobro, J. A. Thorium(IV) Phosphate-Triphosphate: A Valuable Ceramic Material Obtained by Thermal Treatment of a Layered Ammonium-Thorium(IV) Phosphate. Kinetic Analysis of the Transformation. *Ceram. Int.* **2017**, *43*, 10776–10783, https://doi.org/10.1016/j.ceramint.2017.05.091.
5. Zhu, X.; Mochiku, T.; Fujii, H.; Tang, K.; Hu, Y.; Huang, Z.; Luo, B.; Ozawa, K.; Wang, L. A New Sodium Iron Phosphate as a Stable High-Rate Cathode Material for Sodium Ion Batteries. *Nano Res.* **2018**, *11*, 6197–

6205, https://doi.org/10.1007/s12274-018-2139-0.
6. Marouani, H. Chemical Preparations, Crystal Data for Monophosphates and Condensed Phosphates Associated to Manganese and IR Studies of Their Anions. *Int. J. Emerg. Trends Eng. Res.* **2020**, *8*, 4784–4798, https://doi.org/10.30534/ijeter/2020/116882020.
7. Charaf, A.; Fahim, I.; Tace, E. M.; Tridane, M.; Radid, M.; Belaaouad, S. Physico-chemical studies of $CuNa_3P_3O_{10}.12H_2O$, crystallographic characterization of cuna3p3o10 and quantum chemical calculations of the $P_3O_{10}^{5-}$ion. *Phosphorus Res. Bull.* **2010**, *24*, 83–90, https://doi.org/10.3363/prb.24.83.
8. Kenzhaliyev, B.K.; Lokhova, N.G.; Kvyatkovskaya, M.N.; Baltabekova, Z.A. Thermal Analysis for Determination of Individual REM Phases in Industrial Middling Product. *Int. J. Adv. Sci. Technol.* **2020**, *29*, 01–07.
9. Khaoulaf, R.; Brouzi, K.; Ennaciri, A.; Harcharras, M.; Elhafiane, F. Vibrational Spectra of Dizincate Sodium Triphosphte Nonahydrate $Zn_2NaP_3O_{10}.9H_2O$. *J. Mater. Environ. Sci.* **2017**, *8*, 2884–2893.
10. Lutsko, V., Johansson, G. The Crystal Structure of Trisodium Cadmium Triphosphate $Na_3CdP_3O_{10}.12H_2O$. *Acta Chem. Scand.* **1984**, *38a*, 415–417.
11. Belhabra, M.; Fahim, I.; Atibi, A.; El Kababi, K.; Ouasri, A.; Zerraf, S.; Tridane, M.; Radid, M.; Belaaouad, S. Vibrational Study and Thermal Behavior of Dihydrogenotriphosphate Trihydrate of 4-Aminobenzoic Acid and Its Anhydrous New Form Fertilizer Type NP. *Mediterr. J. Chem.* **2019**, *8*, 270–282, https://doi.org/10.13171/mjc841905308mb.
12. Nagorny, P.G.; Slobodyanik, N.S.; Ushchapivska, T.I.; Lavrik, R.V. Double Phosphates $NaMn_6(P_3O_{10})(P_2O_7)_2$ and $KMn_6(P_3O_{10})(P_2O_7)^{2-}$ Advanced Functional Materials. *Funct. Mater.* **2018**, *25*, 689–694, https://doi.org/10.15407/fm25.04.689.
13. Rezgui, E.; Marzouki, R.; Bani-Fwaz, M.Z.; Ouerfelli, N. A New Triphosphate $TlFeHP_3O_{10}$: Synthesis, Crystal Structure, Tl^+ and Proton Conduction Pathways. *Int. J. Electrochem. Sci.* **2020**, 8512–8526, https://doi.org/10.20964/2020.09.15.
14. Rezgui, E.; Krimi, M.; Marzouki, R.; Ateeg, A.A.; Ouerfelli, N. Synthesis, Crystal Structure, Ca^{2+} and Proton Conduction Pathways of New Triphosphate $Ca_{0.5}FeHP_3O_{10}$. *Int. J. Electrochem. Sci.* **2021**, 151085, https://doi.org/10.20964/2021.01.78.
15. Gao, J.; Liu, X.; Song, L.; Sha, X.; Zhao, P.; Guo, P. Synthesis and Structure of a New Halophosphate $Sr_3P_3O_{10}Cl$ with the Flexible $[P_3O_{10}]^{5-}$ Anions. *Solid State Sci.* **2016**, *55*, 159–163, https://doi.org/10.1016/j.solidstatesciences.2016.03.008.
16. Kandori, K.; Mitsui, M. Synthesis and characterization of ce(iii)-substituted calcium hydroxyapatite particles by forced hydrolysis of $Ca(OH)_2$-$Na_5P_3O_{10}$-$CeCl_3$-mixed solution. *Phosphorus Res. Bull.* **2015**, *30*, 8–14, https://doi.org/10.3363/prb.30.8.
17. Oelkers, E. H.; Montel, J.-M. Phosphates and Nuclear Waste Storage. *Elements* **2008**, *4*, 113–116, https://doi.org/10.2113/GSELEMENTS.4.2.113.
18. EL Makhloufy, S.; Tridane, M.; Majdi, E. M.; Marouani, H.; Zerraf, S.; Belhabra, M.; Cherqaoui, A.; Belaaouad, S. Chemical Preparation, Thermal Behavior and Infrared Studies of the New Cyclotriphosphate Tetrahydrate of Manganese and Distrontium, $MnSr_2(P_3O_9)_2.4H_2O$. *Mediterr. J. Chem.* **2019**, *9*, 280–289, https://doi.org/10.13171/mjc941911141082sem.
19. Bruker. APEX3, SAINT-Plus, XPREP. Bruker AXS Inc., Madison, Wisconsin. *USA*, **2016**.
20. Sheldrick, G. M. No Title. *Acta Crystallogr. Sect. B Struct. Crystallogr. Cryst. Chem.* **2015**, *A71*, 3–8. https://doi.org/10.1107/S2053273314026370
21. Sheldrick, G. M. No Title. *Acta Crystallogr. Sect. C Cryst. Struct. Commun.* **2015**, No. C71, 3–8. https://doi.org/10.1107/S2053229614024218
22. Jouini, O.; Dabbabi, M.; Averbuch-Pouchot, M. T.; Durif, A.; Guitel, J. C. Structure Du Triphosphate de Cuivre(II) et de Trisodium Dodécahydraté, $CuNa_3P_3O_{10}.12H_2O$. *Acta Crystallogr. Sect. C Cryst. Struct. Commun.* **1984**, *40*, 728–730, https://doi.org/10.1107/S0108270184005503.
23. Lutsko, V.; Johansson, G.; Boyce, J. B.; Claeson, T.; Ohtaki, H. The Crystal Structure of Trisodium Cadmium Triphosphate $Na_3CdP_3O_{10}.12H_2O$. *Acta Chem. Scand.* **1984**, *38a*, 415–417, https://doi.org/10.3891/acta.chem.scand.38a-0415.
24. Nieves, M.; Voltolina, D.; Piña, P. Growth and Biomass Production of Tetraselmis Suecica and Dunaliella Tertiolecta in a Standard Medium Added with Three Products of Zeolitic Nature. *Aquac. Eng.* **2005**, *32*, 403–410, https://doi.org/10.1016/j.aquaeng.2004.09.003.
25. Zerraf, S.; Tridane Malika, S.B. Data of Infrared Vibration Spectroscopy of Cyclotriphosphates. *Data Br.* **2019**, *25*, 1–9, https://doi.org/doi.org/10.1016/j.dib.2019.104075.

26. Fahim, I.; Tridane, M.; Belaaouad, S. Physico-Chemical Studies of $MgNa_3P_3O_{10}.12H_2O$. *MATEC Web Conf.* **2013**, *5*, 04035, https://doi.org/10.1051/matecconf/20130504035.
27. Tridane, M.; Fahim, I.; Benmokhtar, S.; Belaaouad, S. Structural Modifications from $NiNa_3P_3O_{10}.12H_2O$ $ToNiNa_3P_3O_{10}$ New Triphosphate during Dehydration Process. *Phosphorus Res. Bull.* **2015**, *30*, 1–7, https://doi.org/10.3363/prb.30.1.
28. Zerraf, S.; Tridane, M.; Belaaouad, S. Interpretation of the IR Spectrum of Manganese Cyclotetraphosphate $Mn_2P_4O_{12}$ and Vibrational Analysis of the Cycle $P_4O_{12}^{4-}$. *Sci. Arena Publ. Spec. J. Chem.* **2019**, *4*, 1–6.
29. Dewar, M.J. ; Thiel, W. États Fondamentaux Des Molécules. 38. La Méthode MNDO. Approximations et Paramètres. *J. l'American Chem. Soc.* **1977**, *99*, 4899–4907. https://doi.org/10.1021/ja00457a004.
30 Oubouaza, R.; Marouani, H.; Zerraf, S.; Belhabra, M.; Ouasri, A.;Tridane, M.; Belaaouad, S. Chemical preparations, crystal data for monophosphates and condensed phosphates associated to strontium and IR studies of their anions. *International Journal of Emerging Trends in Engineering Research (IJETER)* **2020**, *8*, 6587-6598, http://dx.doi.org/10.30534/ijeter/2020/265892020.
31. El Makhloufy,S.; Oubouaza, R.; Ouasri, A. ; Belaaouad,S. X-Ray Diffraction and Infrared Spectroscopy Data Review Analyses of the Calcium Phosphates. *Biointerface Res. Appl. Chem* **2022**, *12*, 732-755, https://doi.org/10.33263/BRIAC121.732755.
32. Oubouaza, R.; Benson, M.; Wojciechowski, J.; Chtita ,S.; Tridane, M.; Belaaouad, S. Synthesis, Crystal Structure, Vibrational Study and DFT Computation of Barium Dihydrogenomonophosphate $Ba(H_2PO_4)_2$. *Biointerface Res. Appl. Chem* **2022**, *12*, 1120 -1133, https://doi.org/10.33263/BRIAC121.11201133.
33. Ouasri, A.; Rhandour, A.; Saadi,M.; El Ammari,L. X-Ray, DSC, TGA-dTGA, and Vibrational Studies of the Propylenediammonium Hexafluorosilicate $NH_3(CH_2)_3NH_3SiF_6$. *Biointerface Res. Appl. Chem* **2021**, *11*, 12618 - 12632, https://doi.org/10.33263/BRIAC115.1261812632.
34. El Adel, L.; Ouasri, A.; Rhandour, A.; Saadi, M.; El Ammari, L.; Hajji, L. Crystal structure, DSC, TGA and electrical studies of Bis (1,12-dodecamethylenediammonium hexachlorobismuthate chloride dihydrate $(C_{12}H_{30}N_2)_2BiCl_6.Cl_2H2O$. *J. Mol. Struct.* **2020**, *1207*, 127806, https://doi.org/10.1016/j.molstruc.2020.127806.
35. Healy, C.; Harvey-Reid, N.C.; Howard, B.I.; Kruger, P.E. Thermal decomposition of hybrid ultramicroporous materials (HUMs). *Dalton Transactions* **2020**, *49*, 17433-17439, https://doi.org/10.1039/D0DT03852K.
36. Dhouib, I.; Ouasri, A.; Guionneau, P.; Pechev, S.; Elaoud, Z. Synthesis, molecular structure, vibrational studies, optical properties and electrical conduction mechanism of the new hybrid compound based on selenate. *Journal of Saudi Chemical Society* **2020**, *24*, 996-1009, https://doi.org/10.1016/j.jscs.2020.10.007.
37. Dhouib, I.; Ouasri, A.; Elaoud, Z. Disordered structures, vibrational spectroscopy, thermal behavior, and electrical properties of two new tetrachlorometallates complexes [(CH3CH2CH2)4N]2MIICl4 with MII = Co and Mn. *Journal of Saudi Chemical Society* **2020**, *24*, 567-583, https://doi.org/10.1016/j.jscs.2020.06.001.
38. Atibi, A.; El Kababi, K.; Belhabra, M.; Zerraf, S.; Tridane, M.; Belaaouad, S. Chemical preparation, crystal structure and vibrational study of a new dihydrogenotriphosphate trihydrate of 4-aminobenzoic acid fertilizer type NP. *Journal of Coordination Chemistry* **2018**, *71*, 1-11, https://doi.org/10.1080/00958972.2018.1528579.
39. Marouani, H.; Tridane, M.; Majdi, El.; Zerraf, S.; Belhabra, M.; Belaaouad, S. Engineering Techniques applied for studies by Infrared vibration, crystallographic characterization and Thermal Behavior of two new cyclotriphosphates. *International Journal of Emerging Trends in Engineering Research* **2020**, *8*, 239-246, https://doi.org/10.30534/ijeter/2020/30812020.
40. Zerraf, S.; Belhabra, M.; Tridane, M.; Belaaouad, S. Chemical Preparation, Thermal Behavior and IR Studies of the New Chromium Diphosphate Hydrate and Crystal structure of its Corresponding Anhydrous. *Biointerface Research in Applied Chemistry* **2021,** *11*, 13412 – 13420, https://doi.org/10.33263/BRIAC115.1341213420.
41. Louër, D.; Louër, M. Méthode d'essais et Erreurs Pour l'indexation Automatique Des Diagrammes de Poudre. *J. Appl. Crystallogr.* **1972**, *5*, 271–275, https://doi.org/10.1107/S0021889872009483.
42. Louër, D.; Vargas, R. Indexation Automatique Des Diagrammes de Poudre Par Dichotomies Successives. *J. Appl. Crystallogr.* **1982**, *15*, 542–545, https://doi.org/10.1107/S0021889882012552.
43. Evain, M. U-FIT: A Cell Parameter Refinement Program. *IMN Nantes*, France, **1992**.
44. Kissinger, H. E. Reaction Kinetics in Differential Thermal Analysis. *Anal. Chem.* **1957**, *29*, 1702–1706, https://doi.org/10.1021/ac60131a045.
45. Akahira, T., Sunose, T. Res. Report Chiba Inst. Technol. *Technol. Sci. Technol*, **1971**, *16*, 22.
46. Ozawa, T. A New Method of Analyzing Thermogravimetric Data. *Bull. Chem. Soc. Jpn.* **1965**, *38*, 1881–1886, https://doi.org/10.1246/bcsj.38.1881.
47. Coats, A. W., Redfern, J. P. Kinetic Parameters from Thermogravimetric Data. *Nature*, **1964**, *201*, 68–69.
48. Van Krevelens, D. W., Hoftijzer, P.J. Kinetics of Gas-Liquid Reaction-General Theory. *Trans I Chem E*

1954, *32*, 83.
49. Boonchom, B. Kinetics and Thermodynamic Properties of the Thermal Decomposition of Manganese Dihydrogenphosphate Dihydrate. *J. Chem. Eng. Data* **2008**, *53*, 1533–1538, https://doi.org/10.1021/je800103w.
50. Vlaev, L.; Nedelchev, N.; Gyurova, K.; Zagorcheva, M. A Comparative Study of Non-Isothermal Kinetics of Decomposition of Calcium Oxalate Monohydrate. *J. Anal. Appl. Pyrolysis* **2008**, *81*, 253–262, https://doi.org/10.1016/j.jaap.2007.12.003.
51. Noisong, P., Danvirutai, C., Srithanratana, T., Boonchom, B. Synthesis, Characterization and Non-Isothermal Decomposition Kinetics of Manganese Hypophosphite Monohydrate. *Solid State Sci.* **2008**, *10*, 1598–1604, https://doi.org/10.1016/j.solidstatesciences.2008.02.020.